Modeling solute-vacancy trapping at oversized solutes and its effect on radiation-induced segregation in Fe–Cr–Ni alloys

M.J. Hackett [a,*], R. Najafabadi [b], G.S. Was [a]

[a] Nuclear Engineering and Radiological Sciences, University of Michigan, Ann Arbor, MI 48109, USA
[b] Lockheed Martin Knolls Atomic Power Laboratory, P.O. Box 1072, Schenectady, NY 12309, USA

ABSTRACT

Rate theory modeling was used to simulate the effects of oversized solute additions on radiation-induced segregation in austenitic stainless steels. The purpose was to understand the effects of a solute-vacancy trapping mechanism on radiation-induced segregation and to define key parameters that most affect segregation behavior. Sensitivity analysis of the model showed the solute-vacancy binding energy to be the most important model parameter. Binding energies from *ab initio* first principles were calculated for oversized solutes of Pt, Ti, Hf and Zr, with energies of 0.31, 0.39, 0.71 and 1.08 eV, respectively. Differences in binding energies, despite similar sizes of the atoms, suggests that the short-range electronic interactions play an important role in determining binding energy. The model results show oversized solutes to be most effective at reducing grain boundary Cr depletion at temperatures of 450–500 °C for a dose rate applicable to proton irradiations. The reduction increases with increasing oversized solute concentration, where it saturates at approximately 0.1 at.%.

© 2009 Elsevier B.V. All rights reserved.

1. Introduction

Radiation-induced segregation (RIS) is the non-equilibrium segregation of alloying elements near grain boundary sinks caused by the diffusion of irradiation-produced point defects. Since RIS is considered to be part of a complex process that increases the susceptibility for irradiation-assisted stress corrosion cracking (IASCC) in light water reactors [1,2], the accurate predication of RIS may lead to reducing IASCC susceptibility in current light water reactors and advanced designs.

One method for suppressing RIS is the addition of oversized solute atoms. Oversized solutes are believed to affect RIS by altering the concentrations of vacancies and interstitials in the matrix by acting as vacancy traps and enhancing recombination with migrating interstitials. The result is a decrease in the defect flux to sinks, including grain boundaries, with a subsequent reduction in RIS.

The solute-vacancy trapping mechanism and its effect on RIS can be modeled with kinetic rate theory. Mansur et al. [3,4] developed a solute-defect trapping model to simulate enhanced recombination. The model included oversized solute trapping of both vacancies and interstitials, even though only one mechanism, either vacancy trapping or interstitial trapping, would be active for a given solute type. The results showed that the effects of radiation damage on void swelling and creep could be reduced given

sufficiently strong solute-defect binding, but the model was applied to just a single-element system (Ni).

Sakaguchi et al. [5] used a similar solute-vacancy trapping mechanism to model RIS in a Fe–Cr–Ni alloy using input parameters from the Perks' model [6]. The authors empirically fit the model to experimental RIS data to estimate binding energies for Zr and Hf at ~0.8 and 1 eV, respectively, while smaller oversized solute atoms like Ti and Nb had binding energies of ~0.25 and 0.4 eV, respectively. Sakaguchi et al. [5] did not address values for some important parameters, namely the interaction volumes for the capture and recombination of vacancies. More importantly, the RIS model failed to establish any basis for the solute-vacancy binding energies or to explain differences between the oversized solute elements.

Allen et al. [7,8] showed a significant improvement in the predictive capabilities of RIS modeling by including composition-dependent diffusion coefficients in the modified inverse Kirkendall (MIK) model. Previous work by Hackett et al. [9] used the MIK model to simulate the effects of both interstitial and vacancy trapping on RIS. The study revealed that the binding energy was the most important parameter to the trapping model and that large binding energies were required for significant reductions in RIS.

The purpose of this study is to incorporate a solute-vacancy trapping mechanism into the MIK model and to provide evidence for solute-vacancy binding energies to explain differences among oversized solutes. The trapping model (MIK-T) parameters are determined by first principles to provide accurate binding energy values in order to assess the validity of the solute-vacancy trapping

mechanism. The model is then exercised as a function of experimental parameters to understand the mechanistic behavior of different solute additions and irradiation conditions on RIS. Finally, the model identifies the temperature range in which solute elements with the largest binding energies will have the maximum effect on RIS.

2. MIK-T model

The processes by which oversized solutes affect RIS are: (1) trapping, whereby freely migrating vacancies are captured by the oversized solute atom, forming a solute-vacancy complex, (2) recombination in which freely migrating interstitials are able to recombine with the bound vacancy when the interstitial enters the recombination volume of the solute-vacancy complex, and (3) release, where bound vacancies are able to dissociate from the solute-vacancy complex before recombination occurs. The ratio of recombination to release rate determines the effectiveness of the oversized solute in altering RIS. This section describes the MIK-T model.

2.1. Model description

The MIK model uses composition-dependent vacancy diffusivities to calculate RIS for a binary or ternary alloy. The model assumes migration energies of interstitial atoms are the same for each solute species, so interstitial migration to grain boundaries has no effect on RIS. The input parameters that formed the basis of the MIK model resulted in good agreement in segregation results between model and experiment. Since alloy and irradiation conditions in this study are very similar to those used by Allen et al. [7,8,10,11], this study uses the parameters developed for the MIK model. The values for these parameters can be found in Ref. [8]. The defect production rate in Ref. [8] has a value of 7×10^{-6} dpa/s with a 20% efficiency as freely migrating defects (effective rate is thus 1.4×10^{-6} dpa/s) to simulate the Frenkel pair production rate of proton irradiations. The freely migrating defect production rate used throughout this work is 1×10^{-6} dpa/s, assuming 100% efficiency of freely migrating defects.

The MIK-T model incorporates the effects of oversized solute additions in a Fe–Cr–Ni alloy through the processes of vacancy trapping, recombination and release. The model does not treat the oversized solute explicitly, for example, by modeling the system as a quaternary alloy, because the required thermodynamic data for Zr or Hf in an austenitic stainless steel are lacking. Our approach assumes that the oversized solute remains immobile during the simulation time, with no oversized solute segregation to grain boundaries or to sinks.

The first three rate equations are for the ternary alloy elements, Fe, Cr and Ni:

$$\frac{\partial C_{Fe}}{\partial t} = -\nabla \cdot J_{Fe}, \tag{1}$$

$$\frac{\partial C_{Cr}}{\partial t} = -\nabla \cdot J_{Cr}, \tag{2}$$

$$\frac{\partial C_{Ni}}{\partial t} = -\nabla \cdot J_{Ni}. \tag{3}$$

These equations describe the time rate of change of the concentrations of Fe, Cr and Ni, in terms of $-\nabla \cdot J_x$, the divergence of the elemental flux, where x represents Fe, Cr or Ni, and J_x is proportional to the concentration gradient with respect to the distance from the grain boundary.

The rate equations for the free vacancy and interstitial concentrations, C_v and C_i, are:

$$\frac{\partial C_v}{\partial t} = -\nabla \cdot J_v + G_{dpa} - K_{iv}(D_i + D_v)C_vC_i - S_vD_v(C_v - C_v^{eq})$$
$$- K_vC^sC_v + \tau_vC_v^s, \tag{4}$$

$$\frac{\partial C_i}{\partial t} = -\nabla \cdot J_i + G_{dpa} - K_{iv}(D_i + D_v)C_vC_i - S_iD_iC_i - R_vC_v^sC_i. \tag{5}$$

In these equations, $-\Delta \cdot J_x$ is the divergence of the defect flux, G_{dpa} is the defect production rate, $K_{iv}(D_i + D_v)C_vC_i$ is the recombination rate of vacancies and interstitials, and $S_vD_v(C_v - C_v^{eq})$ and $S_iD_iC_i$ are the loss rates of vacancies and interstitials to sinks, respectively. The remaining terms of Eqs. (4) and (5) represent the trapping process, where $K_vC^sC_v$ is the trapping rate for freely migrating vacancies, $R_vC_v^sC_i$ is the recombination rate for trapped vacancies with freely migrating interstitials, and $\tau_vC_v^s$ is the release rate of vacancies from trapping sites. As for the individual variables in the equations, K_{iv} is the recombination coefficient, C_v^{eq} is the thermal equilibrium concentration for vacancies, C_v^s is the trapped vacancy concentration, D_x is the diffusion coefficient, C_x is the concentration, and S_x is the sink density, where, x represents the defect type, either vacancies or interstitials.

The solute reaction rate equations in (1)–(3) are coupled to the defect reaction rate equations in (4) and (5) through the divergence of the flux, where

$$J_x = J_i^x + J_v^x, \tag{6}$$

$$J_i = J_{Fe}^i + J_{Cr}^i + J_{Ni}^i, \tag{7}$$

$$J_v = J_{Fe}^v + J_{Cr}^v + J_{Ni}^v. \tag{8}$$

The series of partial differential equations are solved numerically with the aid of the GEAR package of subroutines [12] to obtain concentration profiles of alloying elements as a function of time and distance from the grain boundary.

The trapping process terms require additional detail, and both term and variable definitions are summarized in Table 1. The Table includes reference values for each variable or parameter used in assessing the MIK-T model. As mentioned previously, Equations for the trapping, recombination and release coefficients are given below.

The trapping rate includes the capture coefficient, K_v, defined as:

$$K_v = 4\pi \cdot r_v'D_vN_D. \tag{9}$$

The recombination rate depends on R_v, the recombination coefficient, defined as:

$$R_v = 4\pi \cdot r_i'D_iN_D. \tag{10}$$

Finally, the vacancy release rate includes τ_v, the dissociation coefficient, and describes the rate at which trapped vacancies are released from the oversized solute atom [13], defined as:

$$\tau_v = \frac{D_v}{a_0^2} \exp\left[-\frac{E_v^b}{k_BT}\right]. \tag{11}$$

The MIK-T model contains rate equations for the concentration of solute-vacancy complexes and unbound solute atoms, respectively

$$\frac{\partial C_v^s}{\partial t} = K_vC^sC_v - \tau_vC_v^s - R_vC_v^sC_i, \tag{12}$$

$$\frac{\partial C^s}{\partial t} = -K_vC^sC_v + \tau_vC_v^s + R_vC_v^sC_i. \tag{13}$$

Note that Eq. (10) does not need to be solved because it is not an independent equation. The concentration of unbound solute atoms can be found by:

$$C^s = C_0^s - C_v^s \tag{14}$$

Table 1
Definitions and reference values for trapping mechanism terms and variables in the MIK-T model.

Term/variable	Definition	Reference Value
K_v	Capture rate of vacancies by oversized solutes	(Eq. (6))
R_v	Recombination rate of captured vacancies with freely migrating interstitials	(Eq. (7))
τ_v	Release rate of vacancies from oversized solutes	(Eq. (8))
r'_v	Capture radius for vacancy defects	5×10^{-10} m
r'_i	Recombination radius for trapped vacancies with interstitials	5×10^{-10} m
N_D	Alloy number density	8.5×10^{28} m^3
a_0	Lattice parameter	3.5×10^{-10} m
E_v^b	Oversized solute-vacancy binding energy	Solute-dependent
k_B	Boltzmann's constant	8.62×10^{-5} ev/K
T	Temperature	400 °C
C_0^s	Initial oversized solute concentration	0.1 at.%
C^s	Oversized solute concentration not bound to vacancies, available for trapping	Time and variable dependent

where C_0^s is the initial unbound solute concentration. Note that this model assumes only one trapped vacancy per solute atom.

2.2. Model sensitivity analysis

Sensitivity analysis determines which of the input parameters has the largest effect on grain boundary segregation. Only the trapping parameters introduced to the MIK-T model are examined here, which includes the binding energy, trapping radius and recombination radius.

The sensitivity is defined by the derivative, $\partial C/\partial P$, of the grain boundary concentration as a function of an input parameter, where ∂C is the change in grain boundary concentration and ∂P is the change in the input parameter. Calculation of the sensitivity uses the ratio of the difference in grain boundary concentration and input parameter, $\delta C/\delta P$, where each input parameter is varied by a factor of 10^{-4} about the reference value to find the difference in grain boundary concentration. The variation of $\partial C/\partial P$ is approximated by the following:

$$\frac{\partial C}{\partial P} \approx \frac{\delta C}{\delta P} = \frac{C' - C_{reference}}{P' - P_{reference}}, \qquad (15)$$

where C' is the model-calculated grain boundary concentration, with $C' = C_{reference} + \delta C$, and P' is for the input parameter, with $P' = P_{reference} + \delta P$. The sensitivities are expressed in the form of a significance, S_P^C, which is defined as the fractional change in calculated concentration relative to the fractional change in the input parameter. This method was used by Allen et al.[8] and will be used here for the sake of consistency. The significance is expressed by

$$S_C^P = \frac{C' - C_{reference}}{P' - P_{reference}} \cdot \frac{P_{reference}}{C_{reference}}. \qquad (16)$$

The larger the significance of the input parameter, the more sensitive the model is to that parameter.

The sensitivity calculations are performed for a Fe–15Cr–13Ni ternary alloy with reference conditions consisting of: 10^{-6} dpa/s, 400 °C, 1 dpa, 0.5 at.% oversized solute concentration, 0.5 eV binding energy, and 0.5 nm for the trapping and recombination radii. Results from the sensitivity study, consisting of the significance values for the input parameters, are given in Table 2. According to the analysis, the most sensitive of the three input parameters is the solute-vacancy binding energy. With a significance of 0.22 for Cr and 0.32 for Ni at 400 °C, the sensitivity is a factor of seven times higher than the trapping or recombination radius.

Comparing the significance values of Table 2 to those calculated for the MIK model [8], the authors found that vacancy migration energies for Cr and Ni had a significance of 57 and −52, respectively, at 400 °C for a Ni–18Cr–9Fe alloy at 0.5 dpa. The vacancy migration energies have significance values that are two orders of magnitude higher relative to the input parameters of the MIK-T model. The reason for the differences in magnitude lies in the importance of the input parameters to the vacancy migration energy. The MIK model was highly sensitive to vacancy migration energy [8]. Since the MIK model has many variables that affect the composition-dependent vacancy migration energy directly, these input parameters also had a large significance. On the other hand, input parameters that have no effect on vacancy migration energy, like dislocation density or interstitial jump frequency, have very small significance values. The MIK-T model parameters have low significance because they do not affect vacancy migration energy, though the low significance does not mean the trapping process is ineffective at changing grain boundary segregation.

The importance of the sensitivity study is twofold. First, the study identified the vacancy binding energy as the most important variable in the trapping process. Accurate values for this input parameter are critical. Second, even with the higher significance of the binding energy, the sensitivity of the input parameters is low enough that some uncertainty in the values will have minimal impact upon the RIS results.

2.3. Determination of binding energy

Although the solute-vacancy binding energy is established as the most important parameter in the MIK-T model, values for the binding energy, in addition to the trapping radius and recombination radius, were previously unknown. Others have estimated binding energies by back-calculating their value based on experimental RIS data [3–5,14]. But no experiments exist that have directly measured these parameters. Therefore, the quantitative

Table 2
Changes in grain boundary concentration and the significance of MIK-T model input parameters at 400 °C at 1 dpa after changing the input values by a factor of 10^{-4}.

Input	Reference value	Change in value	Dose (dpa)	$\Delta_{Conc.}$ at GB (at.%)		Significance	
				Cr	Ni	Cr	Ni
E_v^b	0.5 eV	5×10^{-5} eV	1	2.5×10^{-4}	-6.1×10^{-4}	**0.22**	**−0.32**
r'_v	5×10^{-10} m	5×10^{-14} m	1	3.0×10^{-5}	-7.4×10^{-5}	**0.03**	**−0.04**
r'_i	5×10^{-10} m	5×10^{-14} m	1	3.1×10^{-5}	-7.6×10^{-5}	**0.03**	**−0.04**

method of first principles calculations by the Vienna *Ab initio* Simulation Package (VASP) code [15–18] is used to determine the magnitude of these parameters.

First principles calculations of solute-vacancy binding energy for Zr or Hf in fcc Fe with no spin polarization have been described in detail in reference [19] using the direct method. The direct method compares two energies, that of the solute and vacancy sitting on first nearest-neighbor sites and that of the solute and vacancy as far apart as possible in the cell considering the periodic boundary conditions. The farthest separation possible from a vacancy in a cubic 108 atom simulation cell is an 11th nearest-neighbor (nn), which, in the ideal lattice (no relaxation of the fcc positions), gives a separation of $a\sqrt{11/2}$, where a is the lattice constant. The direct method is an approximation of the binding energy since even at a separation distance of the 11th nn, the solute and vacancy may still interact with each other.

The indirect method is generally considered the more accurate method for calculating solute-vacancy binding energy because it does not include the interaction between strain fields associate with the solute and vacancy when the are $a\sqrt{11/2}$ distance apart. The method is described in detail in Ref. [20]. In this method the energy of the vacancy and solute atom are subtracted separately from the energy of the system where they interact as first nearest-neighbors. As the number of atoms in the simulation cell increases the binding energies of the direct and indirect methods should converge.

Binding energies for Zr and Hf from the indirect method are shown in Table 3 as a function of the nn position, including the distance of the nn position to the origin. For the binding energy values shown in the Table, a negative value denotes repulsion interaction between a solute atom and vacancy. Using the indirect method, binding energies are calculated to be 1.08 eV for Zr and 0.71 eV for Hf when the vacancy is a 1st nn to the oversized solute. Interaction energy for Zr and Hf as a function of nn position is shown in Fig. 1. By the 11th nn position, the binding energy for the oversized solutes is close to zero, which represents weak interaction between the vacancy and the solute and indicates that the current cell size (108 atoms) for the calculations has fully accounted for the solute-vacancy interactions in determining the binding energy. Some additional calculations for the oversized solutes Ti and Pt were performed, with binding energies of 0.39 eV for Ti and 0.31 eV for Pt, also given in Table 3.

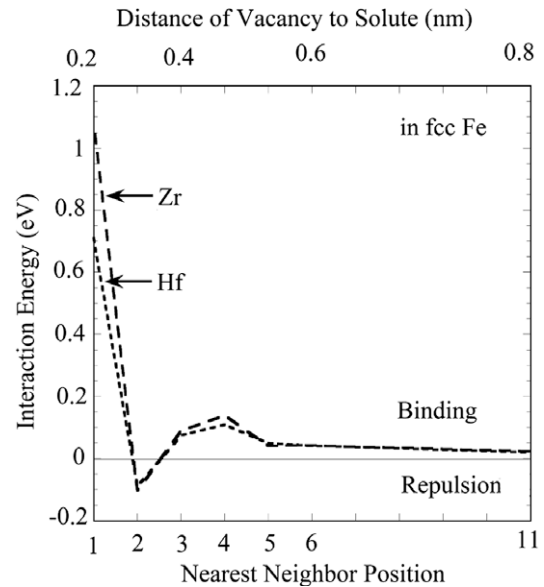### 2.4. Differences between Zr and Hf

Zero-temperature *ab initio* calculations of the lattice parameters for Fe, Zr, Hf, Ti and Pt were performed previously in order to calculate the linear size factors for the oversized solutes in fcc Fe [19]. Values for the calculated lattice parameters are shown in Table 4. The linear size factors can be calculated based on the relationship from King [21], defined as,

$$L_{sf} = \left[(\Omega_{solute}/\Omega_{solvent})^{1/3} - 1 \right] \times 100\% \tag{17}$$

Fig. 1. Calculated interaction energy between an oversized solute (Zr or Hf) and a vacancy as a function of nearest-neighbor position and distance to the oversized solute.

Table 4
Calculated lattice parameters for fcc Fe, Pt, Ti, Hf and Zr and the oversized solute linear size factors in fcc Fe [19].

Atom species	Lattice parameter (nm)	Linear size factor (%)
Fe	0.3448	–
Pt	0.3977	15.3
Ti	0.4090	18.6
Hf	0.4467	29.6
Zr	0.4531	31.4

where Ω_{solute} is the atomic volume of the oversized solute atom and $\Omega_{solvent}$ is the atomic volume of the matrix. Linear size factors have been calculated previously, but were based on atomic volumes of each element's crystal structure (e.g. hcp for Zr and Hf) as opposed to the fcc system.

The linear size factors based on the calculated lattice parameters for each of the oversized solutes are also shown in Table 4. The linear size factors are 15.3% for Pt, 18.6% for Ti, and 31.4% and 29.6% for Zr and Hf, respectively. The similarity in size factors between Zr and Hf reveal that the solute-vacancy binding energy is not simply a function of the elastic strain around the solute atom, as has been proposed in the literature [5,14,21–23]. *Ab initio* calculations show that electronic interactions play a large role in determining the binding energies for oversized solute atoms, shown especially by the large difference in binding energy between Zr and Hf of 1.08 vs. 0.71 eV, respectively, in spite of their similar size factors.

Table 3
Binding energy as a function of nearest-neighbor distance for Zr or Hf in non-spin-polarized Fe using the indirect method.

Vacancy Position	Distance from solute (nm)	Binding energy (eV) – indirect method			
		Zr	Hf	Ti	Pt
1st nn	0.244	1.08	0.71	0.39	0.31
2nd nn	0.345	−0.10	−0.06	–	–
3rd nn	0.422	0.09	0.11	–	–
4th nn	0.488	0.14	0.11	0.04	0.01
5th nn	0.545	0.04	0.08	–	–
6th nn	0.597	0.04	0.08	–	–
11th nn	0.809	0.02	0.02	0.006	0.003

The binding energy of Zr is significantly larger than that for Hf even though their atomic sizes are similar, as shown in Table 4. The reason for the difference in binding energy between Zr and Hf is due to the differences in the electronic effects with the surrounding Fe atoms. System relaxation permits the ions to find the most energetically stable configuration. When placed next to a vacancy defect, the relaxation of Zr toward the vacancy is substantial, as Zr finally rests close to midway between its lattice site and the vacant lattice site. The same relaxation occurs for Hf, but it is less substantial. The Hf ion still rests much closer to its original location on the fcc Fe lattice. The end result is a stronger binding of the solute-vacancy complex for Zr compared to Hf. The solutions for both sets of calculations converged to the same convergence criteria of 1 meV/atom, so the differences in relaxation are not a result of convergence.

2.5. Trapping and recombination radii

The sensitivity analysis used a reference value of 0.5 nm for the trapping and recombination radii. No experimental data exists that could be used to determine the true radius of trapping or recombination for Zr or Hf solute atoms in a Fe–Cr–Ni alloy. However, the binding energy calculations offer some evidence for a realistic value. As shown in Fig. 1, the solute-vacancy interaction energy decreases dramatically when a vacancy moves from a 1st nn position to a position farther from the oversized solute atom. A vacancy in the 2nd nn position has negative interaction energy, indicating repulsion. A vacancy in the 4th nn position is more stable relative to the 2nd or 3rd nn positions, hence the higher interaction energy.

In a fcc lattice with a solute atom at the origin, the 2nd, 3rd, and 4th nn positions are all nearest-neighbors to the 1st nn position. This means any one of them is a possible diffusion path for a vacancy to reach the 1st nn position. The most energetically favorable path for vacancy diffusion is directly from the 4th to the 1st nn position, as evidenced by the relative interaction energies shown in Fig. 1. The distance separating the origin and the 4th nn position, ∼ 0.5 nm, thus makes a logical choice for the radius for vacancy trapping, with the assumption that a diffusing vacancy that reaches the 4th nn position is most likely to then diffuse to the 1st nn position and be captured by the oversized solute.

Interstitial configurations with a solute-vacancy complex were not examined to determine the recombination radius. However, using the same analysis as the preceding paragraph, it may reasonable to assume that the recombination radius has a value similar as the trapping radius. More importantly, some uncertainty in these values will have a negligible effect on calculated RIS because the trapping and recombination radii have low significance values.

3. MIK-T model results and discussion

Having determined values for the key trapping parameter, the MIK-T model is exercised to explore the variations in segregation behavior as a function of irradiation and alloy variables such as temperature, dose, and oversized solute concentration. The purpose is to understand oversized solute effects on segregation behavior as a function of these variables. For variations in temperature and dose, results between the MIK and MIK-T models are compared. All model calculations are for a Fe–15Cr–13Ni alloy. The MIK-T model uses trapping and recombination radii of 0.5 nm with a binding energy of 1.08 eV for Zr and 0.71 eV for Hf.

3.1. Model parameters

The ability of the MIK-T model to accurately describe segregation behavior of oversized solute alloys depends in part on how well the model parameters, including the trapping and recombination radii and binding energy, represent the vacancy trapping process. Neither Mansur et al. [3] nor Sakaguchi et al. [5] give values for the trapping radius or recombination radius used in their models, even though these parameters define the interaction volume for an oversized solute atom. In assessing the MIK-T model, the grain boundary Cr depletion is used as the key dependent variable as it is believed to be the most important aspect of RIS for affecting IASCC susceptibility [1,2]. Fig. 2 plots the amount of grain boundary Cr depletion as a function of the trapping and recombination radii, where both parameters are changed simultaneously from 0 to 1.0 nm. The region from 0 to 0.3 nm is shaded to represent a distance less than the 1st nn position (0.3 nm), since a value less than the 1st nn distance would not be physically meaningful. A value of 0 nm represents a system without trapping.

The majority of the reduction in Cr depletion occurs by the 1st nn distance (0.3 nm). Although interaction volumes for oversized solutes would change dramatically from 0.3 to 1.0 nm, even a small radius of 0.3 nm still has a substantial effect on grain boundary segregation. The MIK-T model uses trapping and recombination radii of 0.5 nm, the difference in Cr depletion between a radius of 0.3 and 1.0 nm is less than 1 at.%. The difference in Cr depletion between a radius 0 and 0.3 nm is more than 3 at% for a Zr-doped alloy. Therefore, modest uncertainty in the value chosen for the trapping and recombination radii of 0.5 nm will not have a substantial effect on the RIS results of the MIK-T model.

In terms of binding energy, Fig. 3 shows the change in grain boundary Cr depletion as a function of the solute-vacancy binding energy. Binding energy values for Pt, Ti, Hf and Zr as calculated from first principles are marked in the Figure. The most important feature is that the larger the binding energy, the more substantial the effect on RIS even up to 1 eV. Sakaguchi et al. [5] claimed from their model that dissociation of solute-vacancy complexes can be ignored when the binding energy is greater than 0.6 eV. The implication is that binding energies above 0.6 eV have a negligible effect on RIS, but this is contrary to the MIK-T model results. In fact, Fig. 4 plots the reaction rates for trapping, release and recombination as a function of binding energy from 0.5 to 1.1 eV. The Figure shows that the recombination rate only becomes substantial relative to the release (dissociation) rate with binding energies above 1 eV. Dissociation of the solute-vacancy complexes continues to be important even with large binding energies.
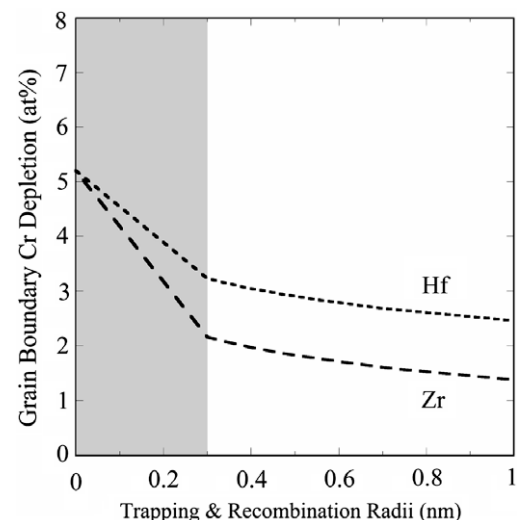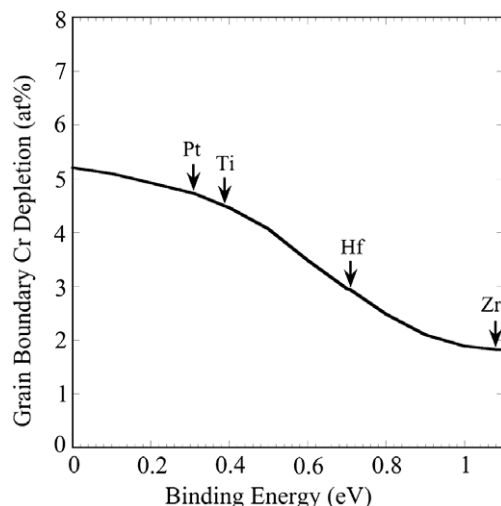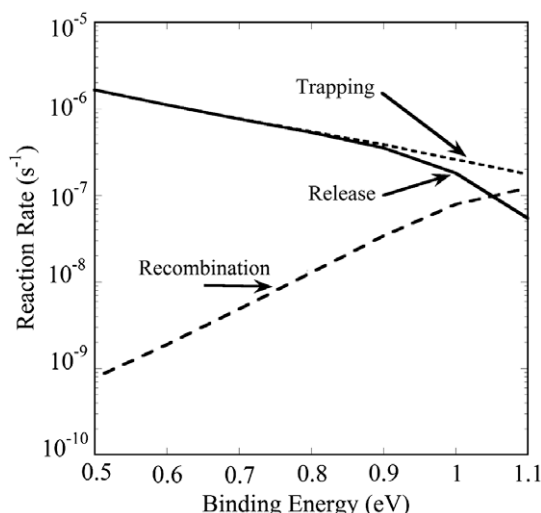

Fig. 2. Grain boundary Cr depletion for the MIK-T model as a function of the trapping and recombination radii varied from 0 to 1.0 nm for Fe–15Cr–13Ni with 0.1 at% Zr or Hf additions at 400 °C, 1×10^{-6} dpa/s and 1 dpa.

Fig. 3. Grain boundary Cr depletion for the MIK-T model as a function of the oversized solute binding energy for Fe–15Cr–13Ni at 400 °C, 1×10^{-6} dpa/s and 1 dpa with 0.1 at% oversized solute. The figure marks the calculated binding energies Pt, Ti, Hf and Zr.
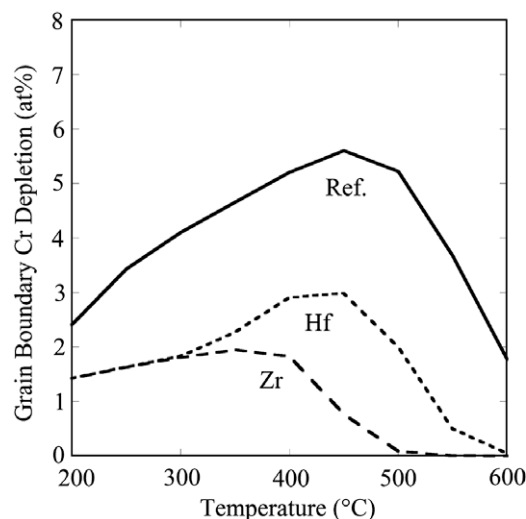

Fig. 5. Grain boundary Cr depletion for the MIK-T model as a function of temperature for Fe–15Cr–13Ni and with 0.1 at% Zr or Hf additions at 1×10^{-6} dpa/s and 1 dpa.

Fig. 4. Calculated trapping, recombination and release rates as a function of the oversized solute binding energy for Fe–15Cr–13Ni at 400 °C, 1×10^{-6} dpa/s and 1 dpa with 0.1 at% oversized solute.

The values for the binding energy and their effect on Cr depletion are consistent with experimental results. Fournier et al. [22] measured a larger reduction in grain boundary segregation for Hf in 316SS than for Pt. Sakaguchi et al. [5] found that Hf and Zr additions to 316SS almost completely suppressed RIS after electron irradiations, while Ti additions were less effective, with some reduction in Ni enrichment but little effect on Cr depletion. The results were similar to those by Kato et al. [14], where Zr or Hf addition to 316L again showed almost complete suppression of RIS after electron irradiation from 400–500 °C, with a less substantial reduction on RIS after Ti addition. These results are consistent with the lower binding energy values calculated for Ti and Pt as compared to Hf and Zr, with the end result that a larger binding energy for the oversized solute means less RIS for the irradiated alloy.

3.2. Irradiation temperature

Fig. 5 shows the amount of grain boundary Cr depletion as a function of irradiation temperature at 1 dpa with a constant dose rate of 10^{-6} dpa/s. Results are shown for the reference case (no oversized solute) and for 0.1 at% Zr or Hf additions. For the reference case, segregation peaks at around 450 °C, with substantially less segregation at the temperature extremes of 200 °C or 600 °C. Maximum segregation occurs for the Hf alloy at 400 °C, and for the Zr alloy at 350 °C. There is almost no segregation at temperatures of 500 °C or higher for the Zr alloy. For the Hf alloy, segregation drops to zero at temperatures of 600 °C or higher. At low temperature, point defect diffusivity is very low, so RIS is also low. Consequently, the difference between the MIK and MIK-T models is small. The difference between models is also small at high temperatures, except that here, point defect diffusivity is large enough that a concentration gradient at the grain boundary does not develop.

Several features of Fig. 5 are noteworthy. At temperatures of less than 300 °C, there is no difference in segregation between Zr and Hf. The difference between Zr and Hf increases from 300 to 500 °C, but by 600 °C the amounts of segregation are again similar. These features of segregation for Zr and Hf can be understood by examining the reaction rates of the MIK-T model.
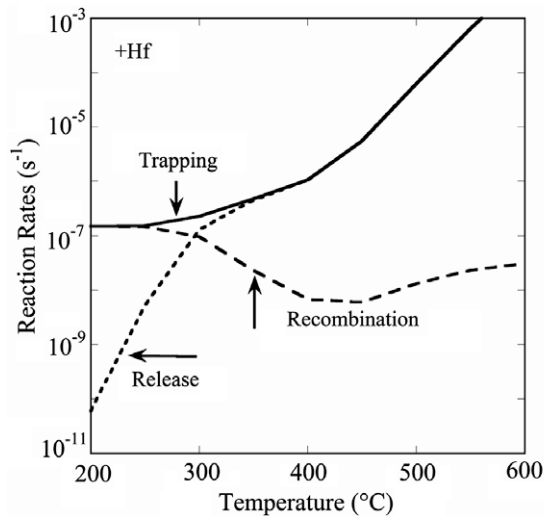
The reaction rates near the grain boundary for vacancy trapping, trapped vacancy recombination and trapped vacancy release are shown in Fig. 6 for Zr and Fig. 7 for Hf. Each Figure shows that recombination dominates at low temperature and the release of trapped vacancies dominates at high temperature. At steady-state, the sum of recombination and release is equal to the rate of trapping.

Below 300 °C trapping rates are identical for Zr and Hf because they are controlled by the trapping radius, which is the same for both Zr and Hf at 0.5 nm. The recombination radius is also the same for Zr and Hf, at 0.5 nm. Differences between Zr and Hf arise only in the rate of release, and at low temperature, the release rate is negligible compared to the recombination rate. Since the binding energy difference between Zr and Hf is irrelevant, and the recombination rates for Zr and Hf are the same, then the reduction in Cr depletion is also the same.

At higher temperatures, the release rate becomes substantial and for Hf, the rate is higher than it is for Zr because of the lower binding energy for Hf. The result is that the recombination rate and the reduction in Cr depletion for Hf are less than they are for Zr. Based on these results, Zr should be substantially more effective than Hf at reducing segregation in the intermediate temperature range.
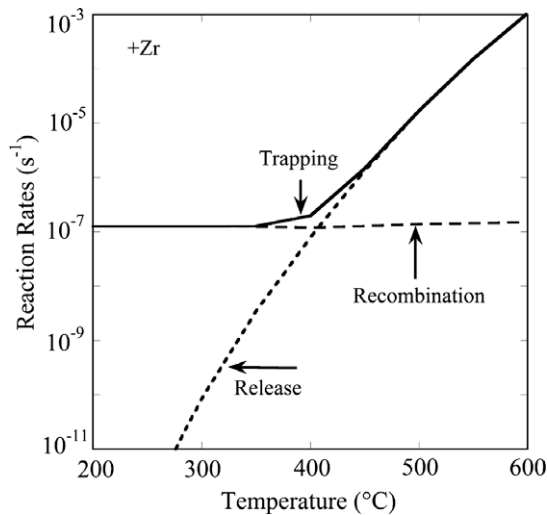
Fig. 6. Calculated reaction rates as a function of temperature for Fe–15Cr–13Ni with 0.1 at% Zr at 1×10^{-6} dpa/s and 1 dpa.
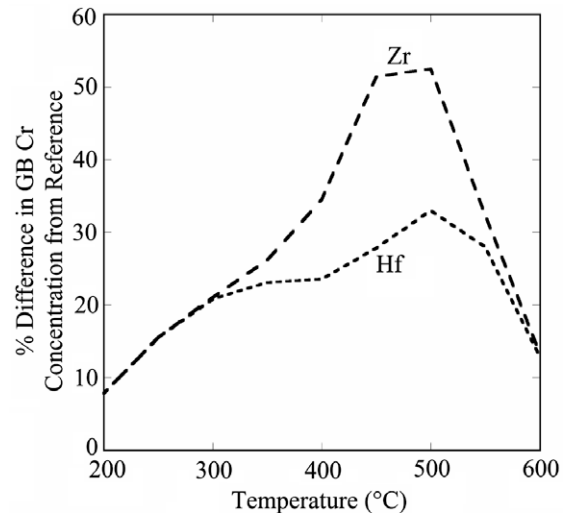

Fig. 8. Calculated percent difference in the grain boundary Cr concentration from the reference alloy as a function temperature for Fe–15Cr–13Ni with 0.1 at% Zr or Hf additions at 1×10^{-6} dpa/s and 1 dpa.

Fig. 7. Calculated reaction rates as a function of temperature for Fe–15Cr–13Ni with 0.1 at% Hf at 1×10^{-6} dpa/s and 1 dpa.

The maximum difference in the grain boundary Cr concentrations between the MIK and MIK-T models occurs between 450 and 500 °C, as shown in Fig. 8. Segregation for the reference alloy has reached a maximum at 450 °C, so both Zr and Hf can cause the largest reduction in segregation around this temperature. While the amount of segregation for the reference alloy is the same at 400 °C and 500 °C, as shown in Fig. 5, the amount of segregation for the oversized solutes at 500 °C is less than at 400 °C. This, too, can be explained by the reaction rates in Figs. 6 and 7 where, although the difference is small, the recombination rate is higher at 500 °C compared to 400 °C for both Zr and Hf, and consequently, the amount of Cr depletion is lower at 500 °C.

3.3. Irradiation dose

Grain boundary Cr depletion for the reference, Zr and Hf alloys are plotted in Fig. 9 as a function of dose up to 10 dpa at 400 °C with 0.1 at% solute at 10^{-6} dpa/s. Segregation changes quickly as a function of dose, with little increase in Cr depletion above 2 dpa. Both Hf and Zr show significant reductions in Cr depletion

in this temperature and dose rate regime. At the intermediate temperature of 400 °C, the difference in Cr depletion between Zr and Hf is controlled by their differences in binding energy.
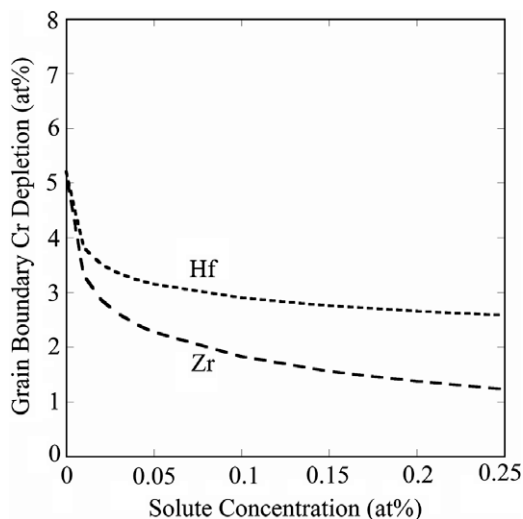
3.4. Oversized solute concentration

The MIK-T model assumes that oversized solute remains in solution for the duration of the simulation time. The assumption is validated by 400 °C p$^+$ irradiation measurements which did not measure any enrichment of oversized solute at grain boundaries [24]. Some evidence existed, however, that oversized solute atoms migrated to carbide precipitates at longer times (> 3 dpa) and gradually lost the vacancy trapping effect. The evidence suggests that simulation of high-dose irradiation experiments would need to include oversized solute diffusion in the rate theory.

Although modeling solute diffusion was outside the scope of the present study, the sensitivity of the MIK-T model to solute concentration provides an understanding of RIS as solute atoms come out
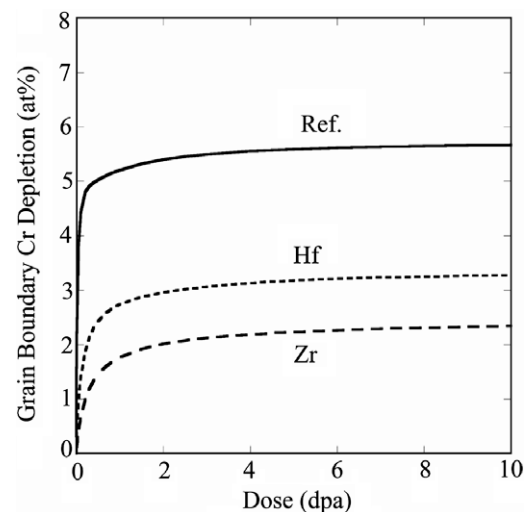

Fig. 9. Grain boundary Cr depletion for the MIK-T model as a function of dose for Fe–15Cr–13Ni and with 0.1 at% Zr or Hf additions at 400 °C, 1×10^{-6} dpa/s and 1 dpa.

Fig. 10. Grain boundary Cr depletion for the MIK-T model as a function of oversized solute concentration for Zr or Hf in Fe–15Cr–13Ni at 400 °C, 1×10^{-6} dpa/s and 1 dpa.

of solution. Fig. 10 shows the grain boundary Cr depletion as a function of Zr and Hf concentration from 0 to 0.25 at% at 400 °C and 1 dpa. Most of the reduction in segregation occurs with solute concentrations less than 0.1 at.%. In a stainless steel with a solute concentration of 0.1 at%, a trapping radius of 1.4 nm would result in overlapping interaction volumes for the oversized solute atoms. For Zr and Hf, a trapping radius of 0.5 nm is more than a third of the value needed for overlapping interaction volume, and 0.1 at% consequently means a relatively high probability for interaction between a vacancy defect and an oversized solute atom. Plotting the recombination rate near the grain boundary for Hf and Zr as a function of solute concentration, Fig. 11 shows that the majority of the change in recombination rate occurs by 0.1 at% solute. Further increases in the solute concentration have a diminishing effect in reducing Cr depletion. The behavior is similar to that in Fig. 2 for Cr depletion as a function of the trapping and recombination radii, where a small value for the input parameter has the majority of the effect on RIS.
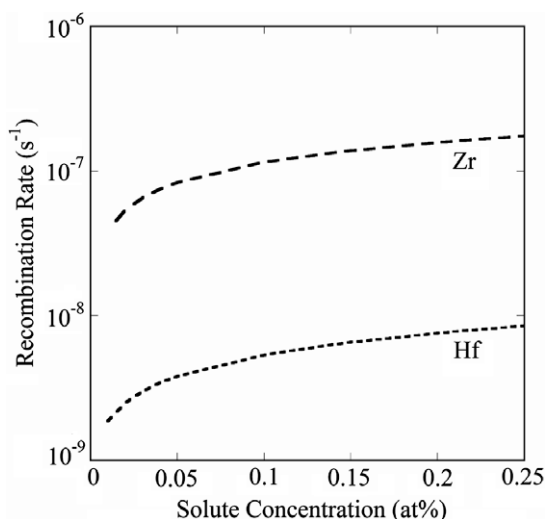
The importance of this result is that small concentrations of an oversized solute can have a large effect on Cr depletion. The result is consistent with work by Shigenaka et al. [25] where a series of Zr alloys were irradiated with He$^+$ ions at 500 °C. The alloys contained varying amounts of Zr. At 0.85 and 3.4 dpa, the effect of 0.41 wt% Zr addition is to reduce Cr depletion by more than 6 wt%. Meanwhile, the difference between alloys with 0.21 wt% Zr and 0.41 wt% Zr is less than 1 wt% Cr. Doubling the amount of Zr in the alloy had only an incremental effect on grain boundary segregation. Based on these results, small concentrations of Zr or Hf in solution in austenitic stainless steels should have the largest impact in substantially reducing the amount of radiation-induced segregation at intermediate temperatures from 300 to 500 °C.

4. Conclusions

The primary conclusion from this work is that oversized solute additions to austenitic stainless steels may cause a significant reduction in grain boundary RIS by enhancing the recombination of point defects in the matrix through a solute-vacancy trapping mechanism. The mechanism is most dependent on the solute-vacancy binding energy. Of the transition elements included in this work, binding energies calculated by first principles show that Zr has the largest binding energy, followed by Hf, Ti and Pt. Zr should, therefore, be most effective at reducing RIS. Contrary to the literature, however, solute-vacancy binding energies are more than just a function of the linear size factor and must include the electronic interactions with nearest-neighbor atoms to fully account for the binding energy. Meanwhile, the trapping mechanism is not strongly dependent on the values for the trapping radius or recombination radius. The oversized solutes have the largest effect on RIS at intermediate temperatures, especially from 450 to 500 °C. Finally, only small concentrations of oversized solute are necessary to cause significant suppression of RIS.

References

[1] G.S. Was, P.L. Andresen, J. Mater. 44 (1992) 8.
[2] G.S. Was, S.M. Bruemmer, J. Nucl. Mater. 216 (1994) 326.
[3] L.K. Mansur, M.H. Yoo, J. Nucl. Mater. 74 (1978) 228.
[4] L.K. Mansur, J. Nucl. Mater. 83 (1979) 109.
[5] N. Sakaguchi, S. Watanabe, H. Takahashi, Nucl. Instrum. Meth. Phys. Res. B 153 (1999) 142.
[6] J.M. Perks, S.M. Murphy, Materials for Nuclear Reactor Core Applications, BNES, London, 1987.
[7] T.R. Allen, G.S. Was, E.A. Kenik, J. Nucl. Mater. 244 (1997) 278.
[8] T.R. Allen, G.S. Was, Acta Mater. 46 (1998) 3679.
[9] M.J. Hackett, G.S. Was, E.P. Simonen, J. ASTM Int. 2 (2005) 1–13.
[10] T.R. Allen, Modeling of Radiation-Induced Segregation in Austenitic Fe–Cr–Ni Alloys, University of Michigan, 1998.
[11] T.R. Allen, J.T. Busby, G.S. Was, E.A. Kenik, J. Nucl. Mater. 255 (1998) 44.
[12] A.C. Hindmarsh, Ordinary Differential Equation System Solver, (UCID-30001 Review 3, Lawrence Livermore Laboratory, December, 1974).
[13] L.K. Mansur, Nucl. Technol. 40 (1978) 5–34.
[14] T. Kato, H. Takahashi, M. Izumiya, J. Nucl. Mater. 189 (1992) 167.
[15] G. Kresse, J. Furthmüller, Phys. Rev. B 54 (1996) 11169.
[16] G. Kresse, J. Furthmüller, Comput. Mater. Sci. 6 (1996) 15.
[17] G. Kresse, J. Hafner, Phys. Rev. B 47 (1993) 558.
[18] G. Kresse, J. Hafner, Phys. Rev. B 49 (1994).

Fig. 11. Calculated recombination rate as a function of oversized solute concentration for Zr or Hf in Fe–15Cr–13Ni at 400 °C, 1×10^{-6} dpa/s and 1 dpa.

[19] M.J. Hackett, J.T. Busby, G.S. Was, Metall. Mater. Trans. A 39 (2007) 218–224.
[20] C. Domain, C.S. Becquart, Phys. Rev. B 65 (2002) 024103.
[21] H.W. King, J. Mater. Sci. 1 (1966) 79.
[22] L. Fournier, B.H. Sencer, G.S. Was, E.P. Simonen, S.M. Bruemmer, J. Nucl. Mater. 321 (2003) 192.
[23] L. Kornblit, A. Ignatiev, J. Nucl. Mater. 126 (1984) 77–78.
[24] M.J. Hackett, R. Najafabadi, G.S. Was, J. Nucl. Mater. 389 (2009) 265.
[25] N. Shigenaka, S. Ono, Y. Isobe, T. Hashimoto, H. Fujimori, S. Uchida, J. Nucl. Sci. Technol. 33 (1996) 577.